



Cite this: *J. Mater. Chem. C*, 2019,
7, 11858

Stacking induced indirect-to-direct bandgap transition in layered group-IV monochalcogenides for ideal optoelectronics[†]

Ji-Hui Yang  *^a and Xin-Gao Gong^{ab}

Ideal optoelectronic semiconductors, with suitable direct bandgaps, high optical absorptions, low carrier effective masses, high mobility, low cost, and high stability, have been long sought after during the past few decades. The recent emergence of layered systems opens an alternative door for this search with novel band structure engineering avenues beyond traditional strategies such as strain, alloying and atomic transmutation. However, ideal layered materials for optoelectronics are rarely reported. Here, we report successful non-traditional band structure engineering in naturally-existing layered group-IV monochalcogenides MX (M = Ge, and Sn; X = S, and Se) by finding that stacking can induce indirect-to-direct bandgap transition in MX bilayers due to interlayer interactions. We identify a family of MX bilayers with direct bandgaps ranging from 1.10 eV to 2.20 eV. While these bilayers have nearly similar energetic stabilities as the bulk-derived ground state bilayers, they show superb electronic properties such as high optical absorption, low exciton binding energies, small carrier effective masses and high mobility, making them ideal candidates with better properties than any currently existing materials for optoelectronic applications. Our work shows that layered systems can have additional and unique degrees of freedom beyond the traditional ones for band structure engineering, thus providing new opportunities for the optoelectronic community.

Received 26th July 2019,
Accepted 2nd September 2019

DOI: 10.1039/c9tc04085d

rsc.li/materials-c

Introduction

By converting light into electric current or *vice versa*, optoelectronic materials play important roles in solar energy harvesting and green lighting and are widely used for solar cells, light-emitting diodes (LEDs), lasers, and photo detectors. For an ideal optoelectronic material, the following general requirements should be satisfied: (1) it should have an appropriate size of optical bandgap. For solar cell applications, the bandgap should sit in the range of 0.8–2.0 eV to make sure that the theoretical energy conversion efficiency is larger than 25% according to the Shockley–Queisser limit.¹ For LEDs, the bandgap should be direct and match the color of the emitted light. (2) It should have high optical absorption efficiency or high radiative recombination rate. For this requirement, direct bandgaps are more preferable than indirect ones. (3) The material

should have good stability and be composed of non-toxic and earth-abundant elements. (4) The material should have good mobility and thus carriers can be easily injected or extracted to yield a high efficiency. Besides, the fabrication cost of optoelectronic materials should be low for large-scale and commercial applications. Currently, most of the optoelectronic materials are three-dimensional (3D) systems, including crystalline Si, CdTe,² Cu(In,Ga)Se₂ (CIGS),^{3,4} Cu₂ZnSn(S,Se)₄ (CZTSSe),^{5,6} and MAPbI₃ for solar cells,^{7–9} and GaAs, and GaN for LEDs. However, all these materials have their own challenges that are difficult to overcome so far. For example, crystalline Si has an indirect bandgap;¹⁰ CdTe contains toxic element Cd;^{11,12} CIGS needs rare element In;^{13,14} CZTSSe has low efficiencies due to a large amount of native lattice defects and a small band bending;¹⁵ MAPbI₃ has poor stability;^{16–18} GaAs and GaN have high fabrication costs due to the molecular beam epitaxial growth conditions. As a result, searching for and/or designing new optoelectronic materials with ideal properties has always been a critical issue and of great importance for this field.

Recently, layered materials have attracted much interest and they show some advantages compared to common 3D systems for optoelectronic applications, one of which is that the properties of layered materials can be more flexibly manipulated by novel avenues such as layer thicknesses, stacking sequences, substrates, and electrostatic gating, in comparison with traditional

^a Department of Physics, Key Laboratory for Computational Science (MOE), State Key Laboratory of Surface Physics, Fudan University, Shanghai 200433, China.
E-mail: jhyang04@fudan.edu.cn

^b Collaborative Innovation Center of Advanced Microstructures, Nanjing 210093, Jiangsu, China

† Electronic supplementary information (ESI) available: Structural parameters of MX monolayers and bilayers, VBM alignments between SnSe monolayer and bilayers as well as optical properties, band edge partial charge densities and density of states of MX bilayers. See DOI: 10.1039/c9tc04085d

strategies like strain, alloying and atomic transmutation in 3D systems. For example, the bandgaps of transition metal dichalcogenides (TMDs) undergo an indirect-to-direct transition from few-layer to monolayer.^{19,20} The bandgaps of black phosphorus can be tuned from 1.60 eV in the monolayer to 0.30 eV in the bulk while remaining direct^{21–23} and a ~3% in-plane strain can change the bandgap of phosphorene from direct to indirect.²⁴ The direct bandgap of bilayer black phosphorus can vary from 0.78 to 1.04 eV with different stacking orders²⁵ and the anisotropy of the electronic structure and optical transitions in 90° twisted bilayer black phosphorus can be tuned by gating.²⁶ In addition to the flexibility of manipulating the electronic properties, layered materials also have the advantage of high efficiencies for optoelectronic applications as only atomically thin films. For example, solar cells based on TMD monolayers have energy conversion efficiencies of ~0.5%²⁷ and ultrathin (~1 nm) solar cells based on a stack of graphene and MoS₂ have an energy conversion efficiency of up to 1%.²⁸ Compared to conventional three-dimensional solar cell materials, monolayer solar cells do have very low efficiency so far, mainly attributed to the low optical absorption of atomically thin semiconductors along the vertical direction. However, considering that monolayer solar cells are only atomically thin and can be produced at very low cost and in large areas, the energy conversion efficiency is already very significant. In other words, if the low optical absorption is overcome, for example, by stacking monolayer solar cells vertically while keeping fundamental properties of monolayers unchanged, *i.e.*, using BN to separate each monolayer, high optical absorption can be obtained using just tens of monolayers, that is, a total material thickness of about 100 nm. Compared to the material amount used in traditional solar cells (several-micrometer thickness at least), monolayer solar cells could be very competitive for low cost.²⁸ Besides, the lacking of dangling bonds in layered material surfaces is expected to be helpful for optoelectronic performance by minimizing the non-radiative carrier recombination at surfaces and interfaces.²⁹ In addition, solar cells and light-emitting diodes made of monolayers can have good flexibility for folding, manifesting them for future solar, lighting and display technologies. Despite layered materials having advantages for optoelectronic applications, the ideal systems are yet to be discovered or designed since monolayer TMDs have relatively large carrier effective masses,^{30,31} low carrier mobility,^{32–34} and large exciton binding energies³⁵ and phosphorene has poor environmental stability^{36,37} and large exciton binding energy.^{38,39} Nevertheless, it is still worth expecting to engineer existing layered systems *via* non-traditional methods such as stacking manipulation in order to find ideal optoelectronic materials.

In this work, we consider to engineer the analogues of phosphorene, group-IV monochalcogenides MXs (M = Ge, and Sn and X = S, and Se) for optoelectronics using non-traditional band structure engineering methods. The reasons are as follows. First, bulk MXs naturally exist in nature and they are composed of relatively earth-abundant and low-toxic elements.^{40,41} Second, bulk MXs have experimentally shown large optical absorption coefficients and they are already good candidates for solar cells²⁹ but they all have indirect bandgaps. Third, MX monolayers like

SnSe are already experimentally synthesized with large areas.⁴² Fourth, similar to phosphorene, MX monolayers have relatively small carrier effective masses and high mobility,⁴³ which is good for carrier extraction and injection. Besides, MX monolayers have relatively small exciton binding energies^{43,44} and much better environmental stabilities than phosphorene.⁴⁰ The challenge is that, MX monolayers generally keep the indirect bandgap nature of their bulks except monolayer GeSe.^{43,44} In addition, the bandgaps of GeS and SnS monolayers are too large for solar cells.⁴³ Therefore, to become the ideal candidates for optoelectronic applications, the electronic properties of MX systems in general need to be engineered for direct and suitable bandgaps.

Taking the advantage of great flexibility for manipulating the electronic properties of layered materials and noticing that MX monolayers have nearly degenerated multivalleys of conduction or valence bands, we consider engineering MX systems by stacking two MX monolayers into bilayers, in which the relative eigenvalue positions of the band edge states can be very sensitive to the stacking orders. We find that, while the ground states of MX bilayers with the bulk-derived AB'-stacking order have indirect bandgaps as their bulks and monolayers, a novel AB stacking induces indirect-to-direct bandgap transitions due to appropriate interlayer interactions. More importantly, the AB stacking structures have nearly the same energetic stabilities as the ground AB'-stacking structures with the total energies only a few meV per atom higher, indicating that the novel AB stacking is very likely to be realized. Other stacking orders with the energies slightly higher than AB'-stacking can also make some MX bilayers direct bandgap semiconductors. Besides, due to the interlayer interactions, the bandgaps of MXs are generally reduced from monolayers to bilayers. We show that the direct bandgap MX bilayers with bandgap values ranging from 1.10 eV to 2.20 eV have very high optical absorption coefficients due to the strong transitions and high density of states near the band edges, relatively small carrier effective masses and high mobility, and small exciton binding energies, making them promising for single and tandem solar cells as well as low-cost LEDs covering from infrared red to green light with better properties than any currently existing materials. Our work thus demonstrates the success of non-traditional band structure engineering methods in layered systems, which opens an alternative door of searching/designing ideal optoelectronic materials and provides new opportunities for the community.

Calculation methods

We perform our first-principles calculations using density-functional theory (DFT)^{45,46} as implemented in the VASP code.^{47,48} The electron and core interactions are included using the frozen-core projected augmented wave (PAW) approach.⁴⁹ For all structure relaxations, we adopt the generalized gradient approximation (GGA) formulated by Perdew, Burke, and Ernzerhof (PBE)⁵⁰ and the structures are relaxed until the atomic forces are less than 0.001 eV Å⁻¹ and the total energies are converged to 10⁻⁶ eV with the cutoff energy for plane-wave basis functions set to 400 eV.

The van der Waals interactions in MX bilayers are considered using the zero damping DFT-D3 method of Grimme *et al.*⁵¹ After obtaining the equilibrium structures, we calculate the electronic properties of MX bilayers using the Heyd–Scuseria–Ernzerhof (HSE06) hybrid functional⁵² to correct the bandgaps and the band structures are obtained using maximally localized Wannier function methods implemented in the Wannier90 code.⁵³ Spin-orbital coupling (SOC) is implicitly considered for all the cases.

Results and discussion

Structures and electronic structures of MX monolayers

As shown in Fig. 1(a), MX monolayers adopt the phosphorene structure. Here the *x* axis is along the zigzag direction and the *y* axis is along the armchair direction, which applies to all the structures in this work. The optimized structural parameters are detailed in Table S1 in the ESI,[†] and they are in good agreement with previous works.⁴³ Fig. 1(b)–(e) show that the valence band maximum (VBM) states of the four MX monolayers all lie along the Γ –Y direction and the conduction band minimum (CBM) states all lie along the Γ –X direction, except that the CBM of the GeSe monolayer lies along the Γ –Y direction,

making GeSe a direct bandgap semiconductor and the other three MX monolayers indirect bandgap semiconductors. Our calculated electronic structures of MX monolayers based on HSE06 + SOC are in good agreement with the many body quasiparticle bandgaps based on G_0W_0 approximation,^{43,44} justifying that HSE06 + SOC adopted in this work can well describe the MX systems.

We note that, among the four MX monolayers, when the anions change from S to Se, the bandgaps are much decreased and when the cations change from Ge to Sn, the bandgaps are slightly reduced. This can be understood from Fig. 2(a). We find that the VBM states of MX monolayers are the anti-bonding states derived from the cation s and anion p orbital couplings with anion p dominating and the CBM states are mainly cation p-orbitals. From MS to MSe, as the Se 4p orbital is higher than the S 3p orbital, MSe can have much higher VBM states than MS and thus MSe has much smaller bandgaps. From GeX to SnX, on the one hand, the Sn 5s orbital is higher than the Ge 4s orbital and therefore the cation s-anion p coupling is stronger for SnX, resulting in the higher VBM states. On the other hand, the Sn 5p orbital is lower than the Ge 4p orbital due to the strong spin-orbital coupling effect of Sn.⁵⁴ As a result, the CBM states of SnX are lower than those of GeX. Consequently, SnX has smaller bandgaps than GeX. The above analysis is consistent with our calculated band alignments of the four monolayer systems in Fig. 2b.

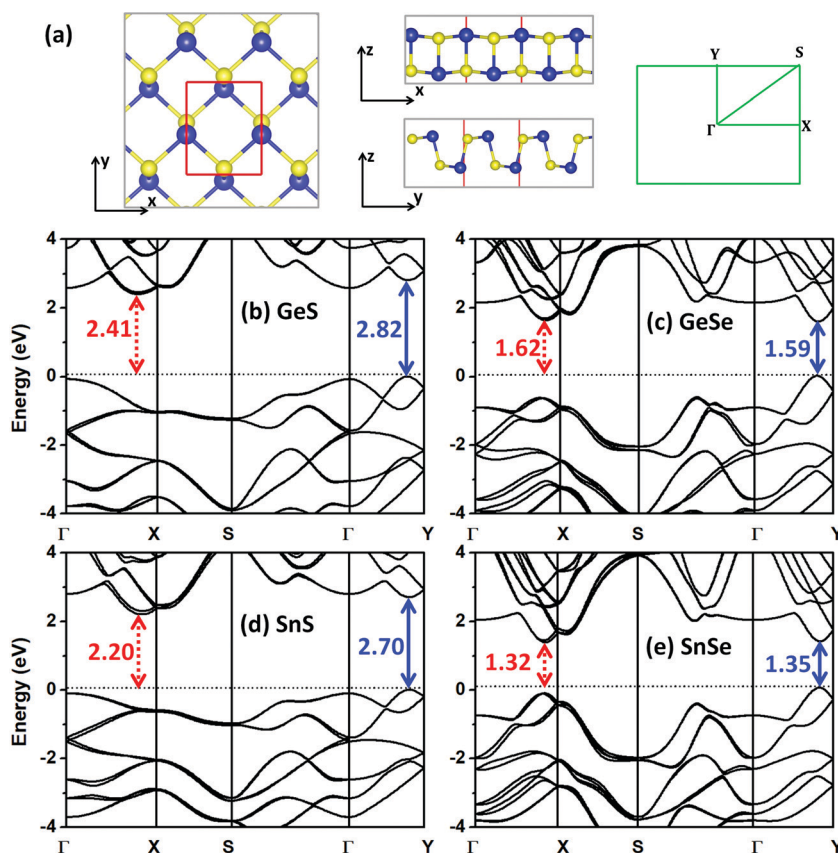


Fig. 1 (a) Top (left panel) and side (middle panel) views of MX monolayers using GeS as an example and k -point path in the first Brillouinzone (right panel). The blue atoms are Ge and the yellow atoms are S. (b–e) Band structures of MX monolayers calculated using HSE06 + SOC. The blue solid lines indicate the direct bandgaps and the red dashed lines indicate indirect bandgaps.

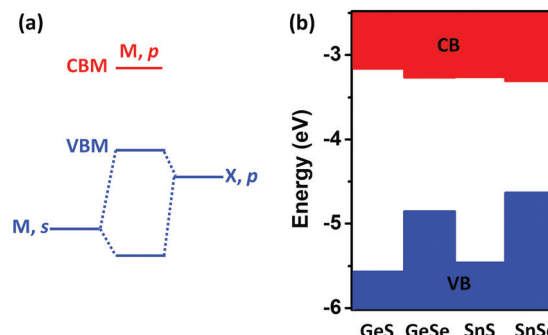


Fig. 2 (a) Diagram showing the formation of VBM and CBM states of MX monolayers. (b) Calculated band alignments between MX monolayers by setting the vacuum level as zero.

Note that, the indirect bandgap nature of GeS, SnS, and SnSe monolayers makes them unsuitable for efficient optoelectronic applications. Besides, the bandgaps of GeS and SnS monolayers are relatively too large for solar cell applications. To engineer the bandgaps of these four systems, previous studies have shown that the in-plane strain can be an effective strategy. For example, the bandgaps of monolayer MX are found to linearly decrease with the compressive in-plane strain but generally they keep indirect.⁵⁵ The tensile in-plane strain, on the other hand, can make some MX direct bandgap semiconductors with increased bandgap values while some MX like GeS still keep indirect bandgaps.⁵⁵ However, the application of in-plane strain is generally limited by the substrates. Due to the usually weak interactions between layered materials and substrates, the in-plane strain that can be applied experimentally is often very small, *i.e.*, less than 1%.^{56,57} Larger in-plane strain will require strong interactions between layered materials and substrates, which will inevitably affect or change the intrinsic material properties. Besides, the presence of a significant amount of defects in MX will make the application of in-plane strain more challenging. To overcome the disadvantages of strain application and achieve efficient band structure engineering of MX systems to make them direct bandgap semiconductors with appropriate bandgap values, herein, we adopt the strategy of stacking two MX monolayers into bilayers with different sequences. As seen

below, through proper stacking, *i.e.*, AB-stacking, all the four MX systems can be turned into direct bandgap semiconductors with optimal bandgap values. Most importantly, the bilayer stacking can be easily achieved with few efforts from MX monolayers.

Structures and electronic structures of MX bilayers

We consider the following stacking orders of MX bilayers. As shown in Fig. 3, in the AA-stacking, the upper layer is just the vertical rigid shift of the bottom layer. The AB-stacking can be viewed as shifting the upper layer of the AA-stacking to make the atoms located above the centers of buckled hexagons in the bottom layer. The AC-stacking can be viewed as left-to-right mirroring the atoms in the upper layer of AA-stacking assuming the mirror is vertically put across the centers of the vertical M–X bonds. The AA', AB', and AC'-stacking are obtained by switching the cations and anions in the upper layers of AA, AB, and AC-stacking, respectively. After structural relaxation, we find that the AC-stacking structures automatically become the AB'-stacking ones while all the other stacking structures are sustained. We compare the energetic stabilities of these stacked structures by considering their total energy differences. As listed in Table 1, the AB'-stacking structures are the most stable ones, which are expected from the fact that, in bulk MX, the stacking order is AB'AB'... along the z direction. The next most stable stacking structures have AB stacking order and their total energies are only a few meV per atom higher than the AB'-stacking structures, indicating that AB-stacking should be achieved very easily. All the other stacking structures, as seen in Table 1, also have relatively small energy differences of less than 30 meV per atom compared to the AB'-stacking, suggesting the large possibilities of their realization.

As for the electronic properties, from monolayers to bilayers, the interlayer interactions can make the electronic states in different monolayers further couple with each other with possible charge transfers or redistribution and the occupied (unoccupied) electronic states can be pushed upward (downward). The stronger the interlayer interactions of these states, the larger the shift these states can have. Depending on the stacking orders, different electronic states can have different interlayer interactions and thus different upward or downward shifts. When this happens in MX systems which have energetically nearly degenerated multivalleys

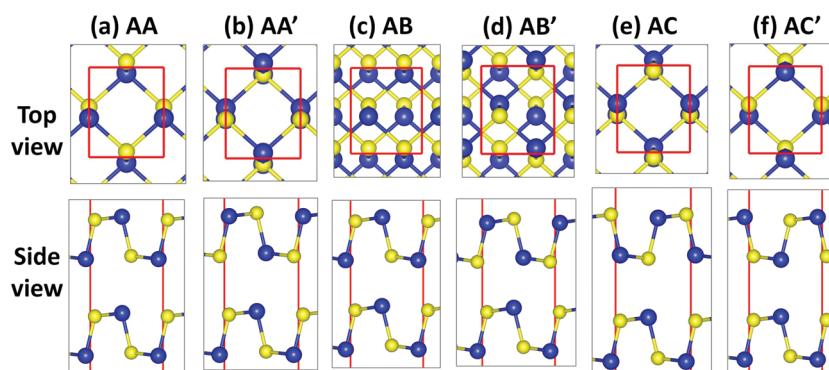


Fig. 3 Top (top panel) and side (bottom panel) views of (a) AA-stacking, (b) AA'-stacking, (c) AB-stacking, (d) AB'-stacking, (e) AC-stacking, and (f) AC'-stacking of MX bilayers using GeS bilayers as examples. The blue atoms are Ge and the yellow atoms are S.

Table 1 Relative energies of different stacking-order MX bilayers with respect to the most stable AB'-stacking structures. The energies are calculated from HSE + SOC and given by meV per atom

Stacking	System			
	GeS	GeSe	SnS	SnSe
AA	17.9	12.8	22.0	21.2
AA'	8.4	5.0	12.0	10.0
AB	4.2	3.2	2.6	4.6
AB'	0	0	0	0
AC'	20.5	18.7	26.4	25.2

of conduction or valence bands, the relative eigenvalue positions of the band edge states can be very sensitive to the stacking orders. In Fig. 4, we show our calculated band structures of these MX bilayers with different stacking orders using the advanced HSE06 functional and considering the SOC effects. As can be seen, the most stable MX bilayers with AB'-stacking all have indirect bandgaps except GeSe, similar to their monolayers. While the VBM states of the MX bilayers with AB'-stacking all lie on the Γ -Y line, the CBM states all sit on the Γ -X line except for GeSe. In contrast to AB'-stacking, all AB-stacking structures have direct bandgaps with both the VBM and CBM states lying on the Γ -Y line.

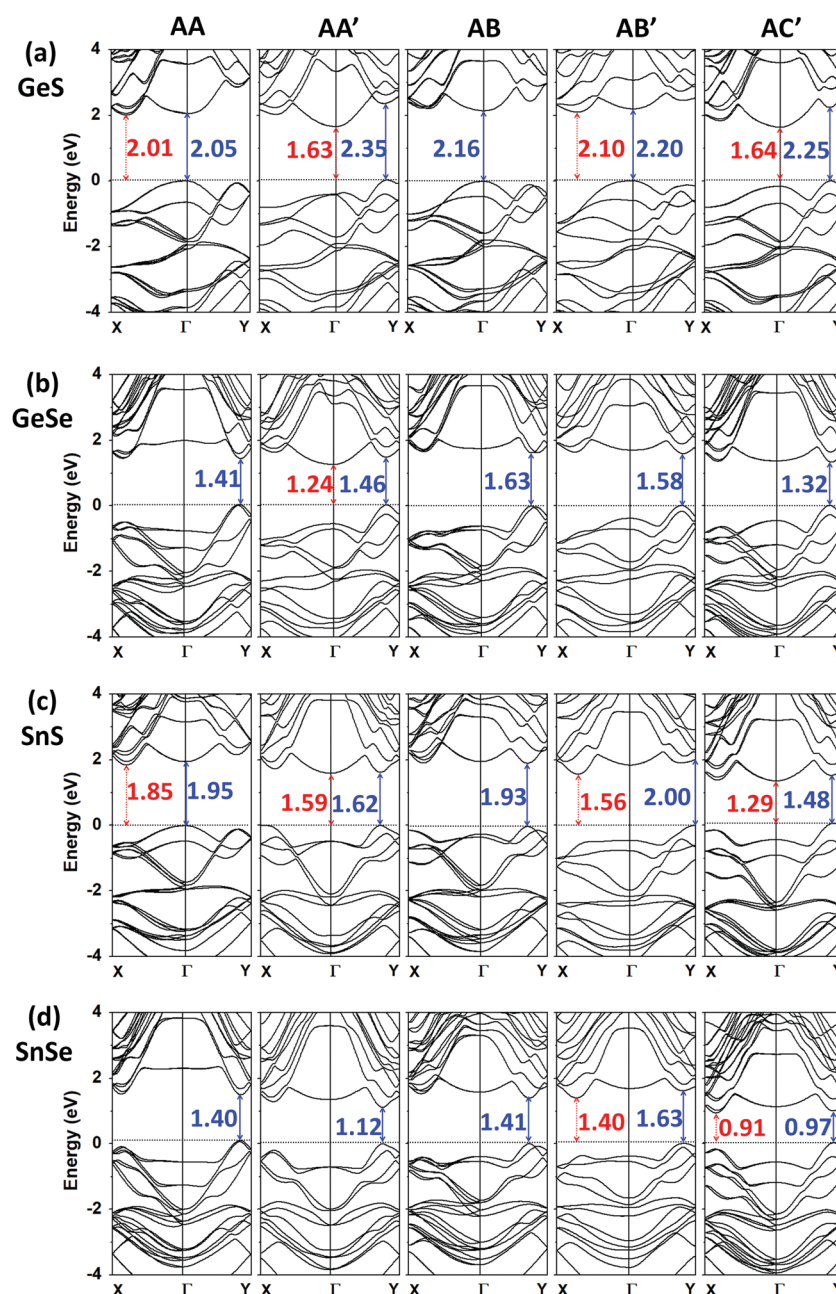


Fig. 4 (a-d) Band structures of MX bilayers with different stacking orders calculated using HSE06 + SOC. The blue solid lines indicate the direct bandgaps and the red dashed lines indicate the indirect bandgaps.

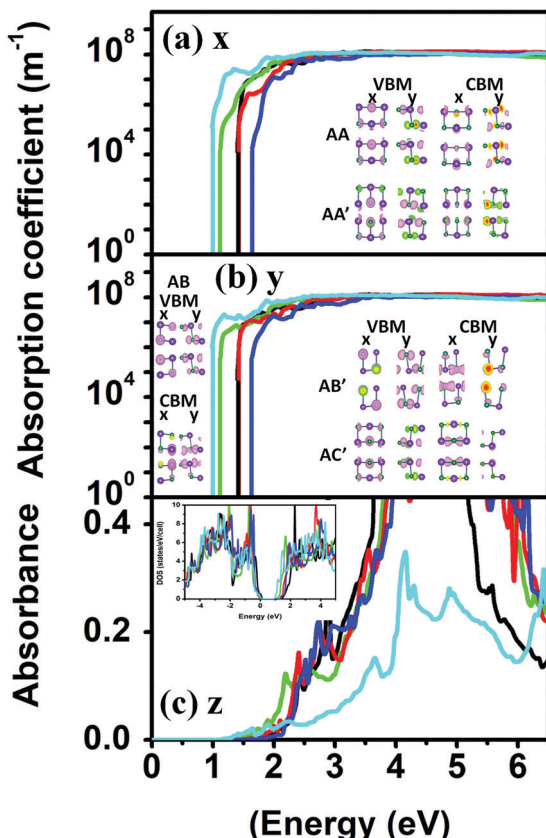


Fig. 5 (a and b) Calculated in-plane optical absorption coefficients and (c) out-of-plane absorbance of SnSe bilayers with different stacking orders. The insets of panels (a and b) indicate the partial charge densities of the VBM and CBM states with the contour set as $0.005 \text{ e } \text{\AA}^{-3}$. The inset of (c) shows the density of states of SnSe bilayers.

The main reason for the indirect-to-direct bandgap transitions from AB'-stacking to AB-stacking can be mainly attributed to the shifts of CBM states from the Γ -X line to Γ -Y line. In the case of AB'-stacking, the CBM states in general have larger interlayer overlap along the x direction, as seen in the insets of Fig. 5. On the other hand, the CBM states have larger interlayer overlap along the y direction in the case of AB-stacking. Consequently, the shifts of CBM states can be qualitatively understood as the following: while the AB'-stacking makes the states along the Γ -X line more strongly interlayer-coupled which pushes part of these states more downward (except for the case of GeSe bilayers), the AB-stacking results in the stronger interlayer coupling for the states along the Γ -Y line, making part of these states become the lowest unoccupied states and leading to the direct bandgaps. Similar situations also happen in GeSe bilayers with AA and AC'-stacking and in SnSe bilayers with AA and AA'-stacking, where the CBM states with larger interlayer overlap along the y direction (as seen in the insets of Fig. 5) lying on the Γ -Y line, making these bilayers direct bandgap semiconductors, as shown in Fig. 4(b) and (d).

From MX monolayers to MX bilayers, the bandgaps of MX systems generally are reduced due to the interlayer interactions except for some cases, *i.e.*, AB and AB' stacked SnSe bilayers, the bandgaps of which are slightly larger than SnSe monolayers.

The exception is mainly due to the reduced Sn s-Se p orbital coupling caused by larger vertical distances between Se and Sn dominating over the interlayer interactions, which leads to the lower VBM states of AB and AB' stacked SnSe bilayers (see Fig. S1 and S2 in the ESI[†] for the VBM alignments between SnSe monolayer and bilayers and bond information). Our calculations show that the bandgaps of MX bilayers with different stacking orders cover a wide range from 0.90 eV to 2.35 eV, which well matches the optimal bandgap requirements for semiconductors to be good photovoltaic absorbers. Besides, the direct bandgap nature of AB-stacking MX bilayers, GeSe bilayers with AA, AB', and AC'-stacking, and SnSe bilayers with AA and AA' stacking, with a bandgap range between 1.10 eV and 2.20 eV, makes them suitable for LEDs covering from infrared to green light.

Optical and electronic transport properties of MX bilayers

The optoelectronic applications require the semiconductors to have not only good bandgap properties but also good optical and transport properties. In the following, we explore the optical and transport properties of MX bilayers with different stacking orders.

Fig. 5 shows our calculated optical properties of MX bilayers, using SnSe as an example (for other MX bilayers, see Fig. S3 in the ESI[†]). As can be seen, the MX bilayers have rather large in-plane optical absorption coefficients in the visible light region reaching 10^6 – 10^8 m^{-1} , which are comparable or even larger than typical photovoltaic absorbers such as GaAs and the recently emerging lead halide perovskites.⁵⁸ The strong optical absorption in MX can be understood from two aspects. First, the band edge transition comes from mixed-(M s, and X p) to M p orbitals, which is similar to that in lead halide perovskites.⁵⁸ The high intra-atomic M s to M p transition probability ensures the high VBM–CBM transition probability. Second, the density of states near the VBM and CBM states in MX bilayers, as seen in the insets of bottom Fig. 5(c) and Fig. S3 (ESI[†]), are high because the VBM and CBM states are mainly composed of degenerate X p and M p bands, respectively. In addition to the strong in-plane optical absorption, the out-of-plane absorption in such thin MX bilayers is also significant. The absorbance of MX bilayers is calculated as $\frac{\omega}{c}\varepsilon_2\Delta z$,²⁸ where ε_2 is the calculated imaginary part of the dielectric function, c is the speed of light, ω is the phonon frequency and Δz is the size of the supercell in the layer-normal direction. As seen in Fig. 5 and Fig. S3 (ESI[†]), the absorbance of MX bilayers can achieve from a few percent to more than 10% in the visible light energy region.

Note that, the exciton effects are not considered in Fig. 5 and Fig. S3 (ESI[†]). For optoelectronic application, excitons can play important roles, *i.e.*, the larger the exciton binding energy, the more difficult it is for electrons and holes to dissociate and thus the more difficult the charge extraction for photovoltaic applications. Due to the weak screening effect in thin layered semiconductors, the exciton binding can be very strong, *i.e.*, the exciton binding energies in monolayer MoS₂ and phosphorene are 0.50 and 0.85 eV, respectively, according to many-body theoretical calculations.⁵⁹ In contrast to these typical layered semiconductors, MX bilayer systems have relatively small exciton binding energies. For example, many-body

theory shows that AB'-stacking GeSe and SnSe bilayers have exciton binding energies of only 0.23 and 0.20 eV, respectively, which are relatively small.⁴⁴ To estimate the binding energies in MX bilayers with different stacking orders, we consider the Wannier–Mott model

in which the exciton binding energy is proportional to $\frac{\bar{M}}{\varepsilon^2}$,⁶⁰ where ε is the macroscopic dielectric constant and \bar{M} is the reduced effective

carrier mass defined as $\frac{1}{\bar{M}} = \frac{1}{m_e^*} + \frac{1}{m_h^*}$ with m_e^* and m_h^* being the effective masses of electrons and holes, respectively. Table 2 lists the carrier effective masses and the reduced effective carrier masses of MX bilayers with different stacking orders. As can be seen, different stacking orders of MX bilayers generally have similar \bar{M} and most of the direct bandgap bilayers have even smaller \bar{M} than the most stable AB'-stacking bilayers, including AA-stacking GeSe and SnSe bilayers, AA'-stacking SnSe bilayers, AB-stacking GeSe, SnS, and SnSe bilayers, and AC'-stacking GeSe bilayers. The smaller \bar{M} indicates that, the exciton binding energies in these direct bandgap bilayers should be smaller than the values in the most stable AB'-stacking bilayers, based on the reasonable assumption that the effect of different stacking orders on the

macroscopic dielectric constants is negligible. We therefore estimate the exciton binding energies in direct bandgap GeSe and SnSe bilayers to be less than 0.20–0.25 eV according to previous many-body calculations.⁴⁴ Such small exciton binding energies compared to the relatively large bandgaps distinguish direct-bandgap MX bilayers from current-known layered semiconductors for optoelectronic applications, especially for photovoltaics.

In addition to optical properties, electronic transport properties of semiconducting materials are also important for optoelectronic applications, as the device performance is strongly related to carrier extraction or injection. As listed in Table 2, the generally small carrier effective masses suggest that MX bilayers can have good transport properties with potentially high carrier mobility. To estimate the mobility, we use the following expression based on deformation potential approximation:^{34,61,62}

$$\mu = \frac{e\hbar^3 C}{k_B T m_e^* m_d (E_1^i)^2},$$

where m_e^* is the carrier effective mass along the transport direction and m_d is the carrier average effective mass determined

Table 2 Calculated electron effective masses (denoted as m_e^*) and hole effective masses (denoted as m_h^*) in MX bilayers with different stacking orders along the orthogonal x and y directions. The normalized carrier effective masses are obtained from $m_e^{*\text{x}} = \sqrt{m_e^{*x} m_e^{*y}}$ and $m_h^{*\text{x}} = \sqrt{m_h^{*x} m_h^{*y}}$, from which the reduced carrier effective masses \bar{M} are obtained. m_0 is the mass of one electron

Effective carrier mass	GeS					GeSe				
	AA	AA'	AB	AB'	AC'	AA	AA'	AB	AB'	AC'
$m_e^{*\text{x}}/m_0$	0.47	1.22	1.53	0.54	1.37	0.20	2.51	0.24	0.16	0.18
$m_e^{*\text{y}}/m_0$	0.23	0.42	0.69	0.30	0.57	0.13	0.53	0.15	0.19	0.15
$m_h^{*\text{x}}/m_0$	4.20	1.10	2.37	6.79	0.93	0.21	0.76	0.24	0.56	0.21
$m_h^{*\text{y}}/m_0$	0.58	0.26	0.61	0.70	0.25	0.22	0.15	0.16	0.20	0.16
\bar{M}/m_0	0.27	0.30	0.55	0.34	0.31	0.09	0.26	0.10	0.11	0.09

Effective carrier mass	SnS					SnSe				
	AA	AA'	AB	AB'	AC'	AA	AA'	AB	AB'	AC'
$m_e^{*\text{x}}/m_0$	0.25	1.21	0.22	0.23	1.09	0.14	0.13	0.17	0.18	0.17
$m_e^{*\text{y}}/m_0$	0.21	0.78	0.17	0.24	0.89	0.11	0.09	0.12	0.17	0.13
$m_h^{*\text{x}}/m_0$	1.96	0.18	0.47	0.50	0.29	0.18	0.11	0.25	0.29	0.14
$m_h^{*\text{y}}/m_0$	0.74	0.17	0.19	1.11	0.25	0.13	0.11	0.13	0.38	0.16
\bar{M}/m_0	0.19	0.15	0.12	0.18	0.21	0.07	0.05	0.08	0.12	0.07

Table 3 Calculated carrier mobility in MX bilayers with different stacking orders along the x and y directions

Mobility ($10^3 \text{ cm}^2 \text{ V}^{-1} \text{ s}^{-1}$)	GeS					GeSe				
	AA	AA'	AB	AB'	AC'	AA	AA'	AB	AB'	AC'
Electron	μ_x	1.21	0.09	0.04	1.04	0.07	1.81	0.11	1.24	1.58
	μ_y	733	1.00	0.13	38.5	4.01	40.2	0.23	7.83	4.42
Hole	μ_x	0.38	0.12	0.06	0.02	0.11	0.60	0.11	0.56	0.23
	μ_y	2.03	0.14	0.40	1.33	0.13	1.55	0.47	0.94	0.27

Mobility ($10^3 \text{ cm}^2 \text{ V}^{-1} \text{ s}^{-1}$)	SnS					SnSe				
	AA	AA'	AB	AB'	AC'	AA	AA'	AB	AB'	AC'
Electron	μ_x	4.22	0.08	1.05	4.63	0.10	3.88	3.15	2.99	17.9
	μ_y	5.29	0.38	62.0	8.68	0.13	2.68	629	1390	21.2
Hole	μ_x	0.09	1.96	0.45	0.06	0.33	0.59	2.36	0.78	0.60
	μ_y	0.07	1.25	0.38	0.04	0.21	0.46	3.12	1.50	0.29

by $m_d = \sqrt{m_x^* m_y^*}$, E_1 represents the deformation potential constant of the VBM for holes or CBM for electrons along the transport direction and C is the elastic modulus of the longitudinal strain in the propagation directions of the longitudinal acoustic wave. This expression is widely used to estimate the carrier mobility in monolayer systems and good agreement between first-principles calculations and experiments are achieved.^{34,61,62} The calculated carrier mobilities of MX bilayers at $T = 300$ K are listed in Table 3. As can be seen, many MX bilayers have anisotropic and relatively high carrier mobility, which can reach the order of 10^3 $\text{cm}^2 \text{V}^{-1} \text{s}^{-1}$ or even higher along the x or y direction for electrons or holes. Interestingly, compared to the most stable AB'-stacking bilayers, all AB-stacking MX bilayers except GeS have higher hole mobility and comparable or even higher electron mobility. Other direct bandgap MX bilayers including AA-stacking GeSe, AA'-stacking SnSe, and AC'-stacking GeSe, also have higher carrier mobility than their most stable AB'-stacking counterparts. The high carrier mobility not only ensures potentially fast carrier extraction or injection but also makes MX bilayers strong candidates for electronic applications such as field effect transistor channel materials.

Screening of MX bilayers for optoelectronic applications

Based on the general material requirements of optoelectronic applications and the above studies of properties of MX bilayers, we screen ideal MX bilayer systems satisfying the following criteria: (1) direct bandgaps for LEDs and direct bandgaps of 0.8–2.0 eV for solar cells, (2) high optical absorption, *i.e.*, $>10^6 \text{ m}^{-1}$, (3) low exciton binding energy, *i.e.*, as low as possible for solar cells and (4) high carrier mobility, *i.e.*, $>10^3 \text{ cm}^2 \text{V}^{-1} \text{s}^{-1}$ for at least one type of carrier along some direction. We find that, all the AB-stacking MX bilayers, AA-stacking GeSe and SnSe, AA'-stacking SnSe, AB-stacking GeSe, and AC'-stacking GeSe with direct bandgaps can be good candidates for red or green light LEDs and all the direct bandgap bilayers except AB-stacking GeS can be ideal candidates for solar cell applications, particularly GeSe and SnSe bilayers with direct bandgaps and small exciton binding energies.

Conclusions

In summary, taking the advantages of the good property nature of MX ($M = \text{Ge}$, and Sn ; $X = \text{S}$, and Se) and the great flexibility for tuning the electronic properties of layered materials, we have demonstrated the success of non-traditional band structure engineering in layered systems. We have found that the stacking order can induce indirect-to-direct bandgap transitions from MX monolayers to bilayers due to proper interlayer interactions. These MX bilayers with different stacking orders show similar energetic stabilities with the ground bulk-derived AB'-stacking order, especially the AB-stacking structures which have the total energies of only a few meV per atom higher. The direct bandgap MX bilayers, including all the AB-stacking MX bilayers, AA-stacking GeSe and SnSe, AA'-stacking SnSe, AB-stacking GeSe, and AC'-stacking GeSe, show very high optical absorption coefficients, and have relatively small carrier effective masses, high

carrier mobility, and relatively small exciton binding energies, making them more suitable than any currently existing materials for optoelectronics. Our work thus provides new opportunities for the optoelectronic community.

Conflicts of interest

The authors declare no competing financial interest.

Acknowledgements

This work was sponsored by Fudan Start-up Funding (JIH1512034) and Shanghai Sailing Program (19YF1403100) and supported by the Supercomputer Center of Fudan University.

Notes and references

- W. Shockley and H. J. Queisser, Detailed balance limit of efficiency of p-n junction solar cells, *J. Appl. Phys.*, 1961, **32**, 510–519.
- J.-H. Yang, W.-J. Yin, J.-S. Park, J. Ma and S.-H. Wei, Review on first-principles study of defect properties of CdTe as a solar cell absorber, *Semicond. Sci. Technol.*, 2016, **31**, 083002.
- J. L. Shay and J. H. Wernick, *Ternary chalcopyrite semiconductors: growth, electronic properties, and applications*, Pergamon Press, Oxford, New York, 1975.
- P. Jackson, D. Hariskos, E. Lotter, S. Paetel, R. Wuerz, R. Menner, W. Wischmann and M. Powalla, New world record efficiency for Cu(In,Ga)Se₂ thin-film solar cells beyond 20%, *Prog. Photovoltaics*, 2011, **19**, 894–897.
- T. K. Todorov, K. B. Reuter and D. B. Mitzi, High efficiency solar cell with earth-abundant liquidprocessed absorber, *Adv. Mater.*, 2010, **22**, E156–E159.
- S. Chen, A. Walsh, X.-G. Gong and S.-H. Wei, Classification of lattice defects in the kesterite Cu₂ZnSnS₄ and Cu₂ZnSnSe₄ earth-abundant solar cell absorbers, *Adv. Mater.*, 2013, **25**, 1522–1539.
- J. Burschka, N. Pellet, S.-J. Moon, R. Humphry-Baker, P. Gao, M. K. Nazeeruddin and M. Grätzel, Sequential deposition as a route to high-performance perovskite-sensitized solar cells, *Nature*, 2013, **499**, 316–319.
- M. M. Lee, J. Teuscher, T. Miyasaka, T. N. Murakami and H. J. Snaith, Efficient hybrid solar cells based on meso-superstructured organometal halide perovskites, *Science*, 2012, **338**, 643–647.
- M. Liu, M. B. Johnston and H. J. Snaith, Efficient planar heterojunction perovskite solar cells by vapour deposition, *Nature*, 2013, **501**, 395–398.
- W. Bludau, A. Onton and W. Heinke, Temperature dependence of the band gap of silicon, *J. Appl. Phys.*, 1974, **45**, 1846–1848.
- J.-H. Yang, S. Chen, W.-J. Yin, X. G. Gong, A. Walsh and S.-H. Wei, Electronic structure and phase stability of MgTe, ZnTe, CdTe, and their alloys in the B3, B4, and B8 structures, *Phys. Rev. B: Condens. Matter Mater. Phys.*, 2009, **79**, 245202.

- 12 A. Shah, P. Torres, R. Tscharner, N. Wyrsch and H. Keppner, Photovoltaic technology: the case for thin-film solar cells, *Science*, 1999, **285**, 692–698.
- 13 V. Fthenakis, W. Wang and H. C. Kim, Life cycle inventory analysis of the production of metals used in photovoltaics, *Renewable Sustainable Energy Rev.*, 2009, **13**, 493–517.
- 14 A. Walsh, S. Chen, S.-H. Wei and X.-G. Gong, Kesterite thin-film solar cells: advances in materials modelling of Cu₂ZnSnS₄, *Adv. Energy Mater.*, 2012, **2**, 400–409.
- 15 Z.-K. Yuan, S. Chen, H. Xiang, X.-G. Gong, A. Walsh, J.-S. Park, I. Repins and S.-H. Wei, Engineering solar cell absorbers by exploring the band alignment and defect disparity: the case of Cu- and Ag-based kesterite compounds, *Adv. Funct. Mater.*, 2015, **25**, 6733–6743.
- 16 J.-H. Yang, W.-J. Yin, J.-S. Park and S.-H. Wei, Fast self-diffusion of ions in CH₃NH₃PbI₃: the interstitial mechanism versus vacancy-assisted mechanism, *J. Mater. Chem. A*, 2016, **4**, 13105–13112.
- 17 B. Conings, J. Drijkoningen, N. Gauquelin, A. Babayigit, J. D'Haen, L. D'Olieslaeger, A. Ethirajan, J. Verbeeck, J. Manca, E. Mosconi, F. D. Angelis and H.-G. Boyen, Intrinsic thermal instability of methylammonium lead trihalide perovskite, *Adv. Energy Mater.*, 2015, **5**, 1500477.
- 18 X.-G. Zhao, J.-H. Yang, Y. Fu, D. Yang, Q. Xu, L. Yu, S.-H. Wei and L. Zhang, Design of lead-free inorganic halide perovskites for solar cells via cation-transmutation, *J. Am. Chem. Soc.*, 2017, **139**, 2630–2638.
- 19 K. F. Mak, C. Lee, J. Hone, J. Shan and T. F. Heinz, Atomically thin MoS₂: a new direct-gap semiconductor, *Phys. Rev. Lett.*, 2010, **105**, 136805.
- 20 A. Splendiani, L. Sun, Y. Zhang, T. Li, J. Kim, C.-Y. Chim, G. Galli and F. Wang, Emerging photoluminescence in monolayer MoS₂, *Nano Lett.*, 2010, **10**, 1271–1275.
- 21 J. Qiao, X. Kong, Z.-X. Hu, F. Yang and W. Ji, High-mobility transport anisotropy and linear dichroism in few-layer black phosphorus, *Nat. Commun.*, 2014, **5**, 4475.
- 22 L. Li, Y. Yu, G. J. Ye, Q. Ge, X. Ou, H. Wu, D. Feng, X. H. Chen and Y. Zhang, Black phosphorus field-effect transistors, *Nat. Nanotechnol.*, 2014, **9**, 372–377.
- 23 L. Li, J. Kim, C. Jin, G. J. Ye, D. Y. Qiu, F. H. da Jornada, Z. Shi, L. Chen, Z. Zhang, F. Yang, K. Watanabe, T. Taniguchi, W. Ren, S. G. Louie, X. H. Chen, Y. Zhang and F. Wang, Direct observation of the layer-dependent electronic structure in phosphorene, *Nat. Nanotechnol.*, 2017, **12**, 21–25.
- 24 H. Liu, A. T. Neal, Z. Zhu, D. Tomanek and P. D. Ye, Phosphorene: an unexpected 2D semiconductor with a high hole mobility, *ACS Nano*, 2014, **8**, 4033–4041.
- 25 J. Dai and X. C. Zeng, Bilayer phosphorene: effect of stacking order on bandgap and its potential applications in thin-film solar cells, *J. Phys. Chem. Lett.*, 2014, **5**, 1289–1293.
- 26 T. Cao, Z. Li, D. Y. Qiu and S. G. Louie, Gate switchable transport and optical anisotropy in 90° twisted bilayer black phosphorus, *Nano Lett.*, 2016, **16**, 5542–5546.
- 27 A. Pospischil, M. M. Furchi and T. Mueller, Solar-energy conversion and light emission in an atomic monolayer p-n diode, *Nat. Nanotechnol.*, 2014, **9**, 257–261.
- 28 M. Bernardi, M. Palummo and J. C. Grossman, Extraordinary sunlight absorption and one nanometer thick photovoltaics using two-dimensional monolayer materials, *Nano Lett.*, 2013, **13**, 3664–3670.
- 29 D.-J. Xue, S.-C. Liu, C.-M. Dai, S. Chen, C. He, L. Zhao, J.-S. Hu and L.-J. Wan, GeSe thin-film solar cells fabricated by self-regulated rapid thermal sublimation, *J. Am. Chem. Soc.*, 2017, **139**, 958–965.
- 30 S. Lebègue and O. Eriksson, Electronic structure of two-dimensional crystals from *ab initio* theory, *Phys. Rev. B: Condens. Matter Mater. Phys.*, 2009, **79**, 115409.
- 31 Y. Yoon, K. Ganapathi and S. Salahuddin, How Good Can Monolayer MoS₂ Transistors Be?, *Nano Lett.*, 2011, **11**, 3768–3773.
- 32 M. S. Fuhrer and J. Hone, Measurement of mobility in dual-gated MoS₂ transistors, *Nat. Nanotechnol.*, 2013, **8**, 146–147.
- 33 B. Radisavljevic and A. Kis, Reply to ‘Measurement of Mobility in Dual-Gated MoS₂ Transistors’, *Nat. Nanotechnol.*, 2013, **8**, 147–148.
- 34 J.-H. Yang, Y. Zhang, W.-J. Yin, X. G. Gong, B. I. Yakobson and S.-H. Wei, Two dimensional sis layers with promising electronic and optoelectronic properties: theoretical prediction, *Nano Lett.*, 2016, **16**, 1110–1117.
- 35 D. Y. Qiu, F. H. da Jornada and S. G. Louie, Optical Spectrum of MoS₂: Many-Body Effects and Diversity of Exciton States, *Phys. Rev. Lett.*, 2013, **111**, 216805.
- 36 S. P. Koenig, R. A. Doganov, H. Schmidt, A. H. Castro Neto and B. Ozilmez, Electric field effect in ultrathin black phosphorus, *Appl. Phys. Lett.*, 2014, **104**, 103106.
- 37 A. Ziletti, A. Carvalho, D. K. Campbell, D. F. Coker and A. H. Castro Neto, Oxygen Defects in Phosphorene, *Phys. Rev. Lett.*, 2015, **114**, 046801.
- 38 Z. Jiang, Z. Liu, Y. Li and W. Duan, Scaling Universality between Band Gap and Exciton Binding Energy of Two-Dimensional Semiconductors, *Phys. Rev. Lett.*, 2017, **118**, 26640.
- 39 L. Seixas, A. S. Rodin, A. Carvalho and A. H. Castro Neto, Exciton binding energies and luminescence of phosphorene under pressure, *Phys. Rev. B: Condens. Matter Mater. Phys.*, 2015, **91**, 115437.
- 40 D. D. Vaughn, R. J. Patel II, M. A. Hickner and R. E. Schaak, Single-Crystal Colloidal Nanosheets of GeS and GeSe, *J. Am. Chem. Soc.*, 2010, **132**, 15170.
- 41 D.-J. Xue, J. Tan, J.-S. Hu, W. Hu, Y.-G. Guo and L.-J. Wan, Anisotropic Photoresponse Properties of Single Micrometer-Sized GeSe Nanosheet, *Adv. Mater.*, 2012, **24**, 4528–4533.
- 42 L. Li, Z. Chen, Y. Hu, X. Wang, T. Zhang, W. Chen and Q. Wang, Single-Layer Single Crystalline SnSe Nanosheets, *J. Am. Chem. Soc.*, 2013, **135**, 1213–1216.
- 43 L. Xu, M. Yang, J. S. Wang and Y. P. Feng, Electronic and optical properties of the monolayer group-IV monochalcogenides MX (M = Ge, Sn X = S, Se, Te), *Phys. Rev. B*, 2017, **95**, 235434.
- 44 G. Shi and E. Kioupakis, Anisotropic Spin Transport and Strong Visible-Light Absorbance in Few-Layer SnSe and GeSe, *Nano Lett.*, 2015, **15**, 6926–6931.
- 45 P. Hohenberg and W. Kohn, Inhomogeneous Electron Gas, *Phys. Rev.*, 1964, **136**, B864–B871.

- 46 W. Kohn and L. J. Sham, Self-Consistent Equations Including Exchange and Correlation Effects, *Phys. Rev.*, 1965, **140**, A1133–A1138.
- 47 G. Kresse and J. Furthmüller, Efficient Iterative Schemes for *ab initio* Total-energy Calculations Using a Plane-wave Basis Set, *Phys. Rev. B: Condens. Matter Mater. Phys.*, 1996, **54**, 11169–11186.
- 48 G. Kresse and J. Furthmüller, Efficiency of *ab initio* Total Energy Calculations for Metals and Semiconductors Using a Plane-Wave Basis Set, *Comput. Mater. Sci.*, 1996, **6**, 15–50.
- 49 G. Kresse and D. Joubert, From Ultrasoft Pseudopotentials to the Projector Augmented-Wave Method, *Phys. Rev. B: Condens. Matter Mater. Phys.*, 1999, **59**, 1758–1775.
- 50 J. P. Perdew, K. Burke and M. Ernzerhof, Generalized Gradient Approximation Made Simple, *Phys. Rev. Lett.*, 1996, **77**, 3865.
- 51 S. Grimme, S. Ehrlich and L. Goerigk, Effect of the damping function in dispersion corrected density functional theory, *J. Comput. Chem.*, 2011, **32**, 1456–1465.
- 52 J. Heyd, G. E. Scuseria and M. Ernzerhof, Hybrid functionals based on a screened Coulomb potential, *J. Chem. Phys.*, 2003, **118**, 8207–8215.
- 53 A. A. Mostofi, J. R. Yates, Y.-S. Lee, I. Souza, D. Vanderbilt and N. Marzari, Wannier90: A tool for Obtaining Maximally-localised Wannier Functions, *Comput. Phys. Commun.*, 2008, **178**, 685–699.
- 54 J.-H. Yang, Q. Yuan and B. I. Yakobson, Chemical Trends of Electronic Properties of Two-Dimensional Halide Perovskites and Their Potential Applications for Electronics and Optoelectronics, *J. Phys. Chem. C*, 2016, **120**, 24682–24687.
- 55 L. Huang, F. Wu and J. Li, Structural anisotropy results in strain-tunable electronic and optical properties in monolayer GeX and SnX (X = S, Se, Te), *J. Chem. Phys.*, 2016, **144**, 114708.
- 56 K. He, C. Poole, K. F. Mak and J. Shan, Experimental Demonstration of Continuous Electronic Structure Tuning via Strain in Atomically Thin MoS₂, *Nano Lett.*, 2013, **13**, 2931–2936.
- 57 O. Frank, M. Mohr, J. Maultzsch, C. Thomsen, I. Riaz, R. Jalil, K. S. Novoselov, G. Tsoukleri, J. Parthenios, K. Papagelis, L. Kavan and C. Gallois, Raman ²D-Band Splitting in Graphene: Theory and Experiment, *ACS Nano*, 2011, **5**, 2231–2239.
- 58 W.-J. Yin, J.-H. Yang, J. Kang, Y. Yan and S.-H. Wei, Halide perovskite materials for solar cells: a theoretical review, *J. Mater. Chem. A*, 2015, **3**, 8926–8942.
- 59 J.-H. Choi, P. Cui, H. Lan and Z. Zhang, Linear Scaling of the Exciton Binding Energy versus the Band Gap of Two-Dimensional Materials, *Phys. Rev. Lett.*, 2015, **115**, 066403.
- 60 L. Ma, J. Dai and X. C. Zeng, Two-Dimensional Single-Layer Organic-Inorganic Hybrid Perovskite Semiconductors, *Adv. Energy Mater.*, 2017, **7**, 1601731.
- 61 G. Fiori and G. Iannaccone, Multiscale Modeling for Graphene-Based Nanoscale Transistors, *Proc. IEEE*, 2013, **101**, 1653.
- 62 S. Bruzzone and G. Fiori, Ab-initio Simulations of Deformation Potentials and Electron Mobility in Chemically Modified Graphene and Two-Dimensional Hexagonal Boron-Nitride, *Appl. Phys. Lett.*, 2011, **99**, 2108.